Accepted Manuscript

Composition Dependent Room Temperature Structure, Electric and Magnetic Properties in Magnetoelectric $Pb(Fe_{1/2}Nb_{1/2})O_3$ - $Pb(Fe_{2/3}W_{1/3})O_3$ Solid-solutions

Shidaling Matteppanavar, Sudhindra Rayaprol, Basavaraj Angadi, Balaram Sahoo

PII: S0925-8388(16)30891-X

DOI: 10.1016/j.jallcom.2016.03.260

Reference: JALCOM 37148

To appear in: *Journal of Alloys and Compounds*

Received Date: 24 January 2016

Revised Date: 22 March 2016

Accepted Date: 29 March 2016

Please cite this article as: S. Matteppanavar, S. Rayaprol, B. Angadi, B. Sahoo, Composition Dependent Room Temperature Structure, Electric and Magnetic Properties in Magnetoelectric $Pb(Fe_{1/2}Nb_{1/2})O_3$ - $Pb(Fe_{2/3}W_{1/3})O_3$ Solid-solutions, *Journal of Alloys and Compounds* (2016), doi: 10.1016/j.jallcom.2016.03.260.

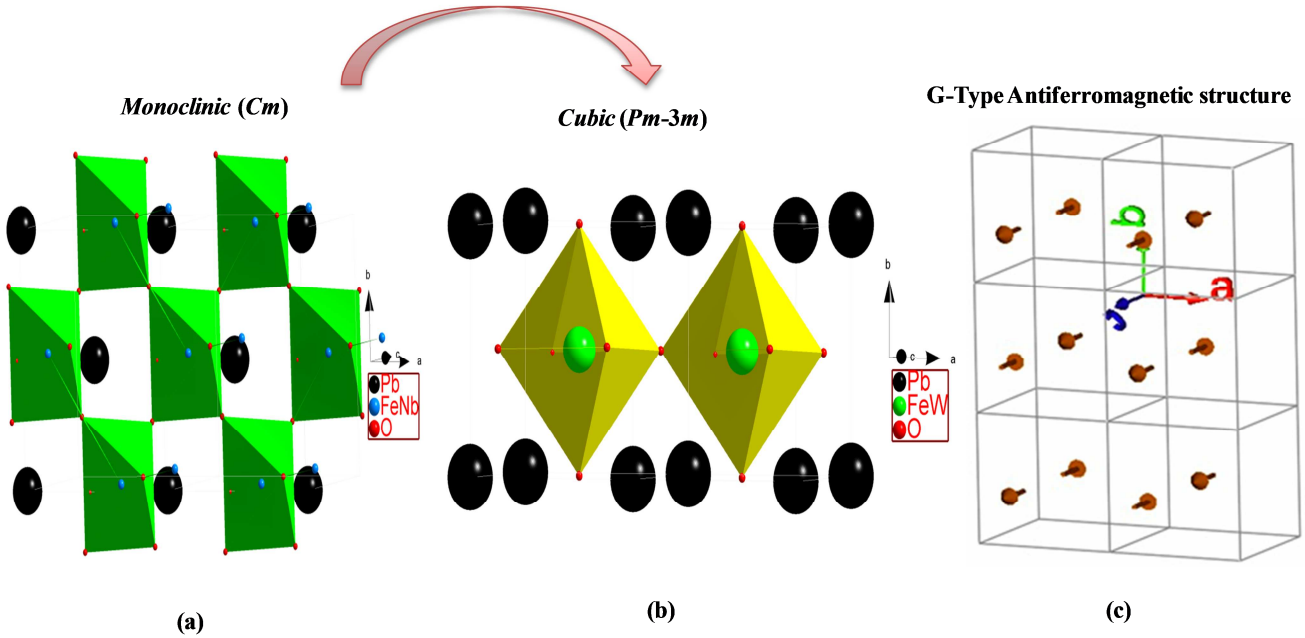

Graphical abstract

Composition Dependent Room Temperature Structure, Electric and Magnetic Properties in Magnetoelectric $Pb(Fe_{1/2}Nb_{1/2})O_3$ - $Pb(Fe_{2/3}W_{1/3})O_3$ Solid-solutions

Shidaling Matteppanavar[1], Sudhindra Rayaprol[2], Basavaraj Angadi[1,*], Balaram Sahoo[3]

[1]*Department of Physics, JB Campus, Bangalore University, Bangalore – 560056, India*

[2]*UGC-DAE-Consortium for Scientific Research, Mumbai Centre, B A R C Campus, Mumbai – 400085, India*

[3]*Materials Research Centre, Indian Institute of Science, Bangalore - 560012, India*

* Corresponding Author:

Dr. Basavaraj Angadi

Assistant Professor

Department of Physics, Bangalore University, Jnanabharathi Campus,

Bengaluru – 560 056, INDIA

Email: brangadi@gmail.com

Phone #: +91-80-2296 1478

Fax #: +91-80-2321 9295

[*] Corresponding Author : e-mail : brangadi@gmail.com

Abstract

We report on the studies of room temperature (RT) crystal structure, electric and magnetic properties of (1-x) $Pb(Fe_{1/2}Nb_{1/2})O_3$ – x $Pb(Fe_{2/3}W_{1/3})O_3$ (PFN_{1-x} – PFW_x) (x = 0.0, 0.2, 0.4, 0.6, 0.8 and 1.0) solid solutions through the measurements of X-ray diffraction, FTIR, scanning electron microscopy (SEM), Neutron diffraction, Raman, Magnetic, Mössbauer and ferroelectric measurements. FTIR spectra showed two main perovskite related transmission bands. The SEM analysis shows an average grain size of 2μm for all the solid solutions. Rietveld refinement was performed on RT X-ray diffraction (XRD) and neutron diffraction (ND), which reveals, the *monoclinic* phase for x = 0.0 with space group *Cm* and *Cubic* phase for x = 1.0 with space group *Pm*-3*m*. In other words, increasing x, the samples exhibit a gradual phase transition from monoclinic to cubic. In addition, the Raman spectroscopy corroborates the change in structural symmetry from monoclinic (*Cm*) to cubic (*Pm*-3*m*) on varying x. The coexistence of both monoclinic and cubic symmetries was observed between x = 0.2 to 0.8. Magnetic measurements shows that, the magnetic phase transition from paramagnetic to antiferromagnetic (AFM) was observed at or above RT for x = 0.6 and above. The magnetic structure was refined using the propagation vector k = (½, ½, ½) and structure was found to be G-type antiferromagnetic. Magnetic properties (*M-H* loops) shows, a weak ferromagnetic behaviour with antiferromagnetic ordering at RT. At RT, x = 0.0 to 0.6 the samples exhibits disordered paramagnetic property but weakly coupled with antiferromagnetic domains. But, x = 0.8 and 1.0 samples show antiferromagnetic and they are weakly coupled with paramagnetic domains**.** The temperature dependent magnetisation (M(T)) confirms, the augmentation of Néel temperature (T_N) from 155 K to 350 K on increasing x. Mössbauer spectroscopy confirms superparamagnetic nature with the presence of Fe in 3+ state and on increasing x, the spectra changes from doublet to sextet. The ferroelectric (P-E) study confirms the existence of ferroelectric ordering with leaky

behaviour. The reasonable ferroelectric loops with antiferromagnetic properties indicate samples with x = 0.2 to 0.6 show good magnetoelectric characteristics and may find applications in multiferroics.

Key words: Multiferroic, Neutron diffraction, Rietveld Refinement, Phase transition and Magnetic structure.

PACS number(s): 77.80.Bh, 75.50.Ee, 75.80.+q

1. INTRODUCTION

Recently, there has been an increased intense research on searching for RT or near RT magnetoelectric multiferroics for both fundamental scientific understanding and to fabricate novel multifunctional devices [1 - 3]. The coexistence both ferromagnetic and ferroelectric orders in single phase multiferroics with ABO_3 - type perovskite structure has been contradicted as the former requires empty d orbitals for the off-centering of B ions in the oxygen octahedral cage, while the latter requires partially filled d orbitals [4]. $Pb(Fe_{1/2}Nb_{1/2})O_3$ (PFN), $Pb(Fe_{1/2}Ta_{1/2})O_3$ (PFT) and $Pb(Fe_{2/3}W_{1/3})O_3$ (PFW) multiferroic compounds belong to $Pb(B'B'')O_3$ type complex perovskite structure family [1–3] [B′-low valence cation (Fe^{3+}), B"-high valence cation (Nb^{5+},Ta^{5+},W^{6+})] and were discovered in the early 1960s [3, 4, 5, 6]. In this family, the Fe^{3+} B' provide unpaired $3d^n$ electrons for magnetic ordering, whereas the distortion introduced by non-magnetic W^{6+} and Nb^{5+} on the B" exhibiting d^0 configuration gives rise to ferroelectric ordering. These complex structured multiferroics show unique large electric polarization/magnetization, high piezoelectric coefficients and reasonably high magneto-electric coupling coefficient; hence they attracted researchers' attention for their potential applications in multifunctional devices. These multiferroics (PFN and PFW) independently have shown to display simultaneously, ferromagnetic and ferroelectric properties below RT and confirm the evidence of ME

coupling experimentally and theoretically. Though PFN and PFW are potential candidates for ME coupling studies, however not at RT. PFN has ferroelectric Curie temperature (T_C) at 350 K and anti-ferromagnetic Neel temperature (T_N) at 155 K. Similarly, PFW has T_C below 200 K and T_N below 350 K [5 - 7]. In order to shift the magnetic ordering temperature in PFN and to achieve the RT multiferroic properties, it is desired to make solid solution of PFW with PFN, due to the similar perovskite structure with small amount of diluting ferroelectricity.

Recently, many researchers have tried to make RT or near RT Pb based ME multiferroics by using the mixed perovskites of PFN, PFW and PFT with $PbZr_{1-x}Ti_xO_3$ (PZT) [8 - 16], due to the existence of rich magnetoelectric and magnetoelastic coupling between them. Among these, PFW-PZT showed unique coupling mechanism and it was studied in some detail both theoretically and experimentally. Recently, Scott et. al. [9] reported in the review article, that the solid solutions of PZT with PFN, PFW and PFT have failed to show magnetoelectric coupling. Also theoretical calculations by Glinchuk et. al. [15 and 16] suggest that there is no bilinear $\alpha_{ij}\ P_iM_j$ magnetoelectric coupling, but all that interaction between P and H is via magnetostriction bM^2S^2 plus electrostriction dP^2S^2 and piezoelectricity $d_{ijk}P_iS_{jk}$. This can produce a useful room-temperature device in which +P switches to zero (not to -P), but it is not strictly a magnetoelectric multiferroic. From the studies, PFN/PFW/PFT – PZT solid solutions are not magnetoelectric multiferroic, because of the bilinear magnetoelectric interaction of form P x M and that E fields and H fields are not at all equivalent switching fields. Instead, switching is quadratic in M (similar to CuO), and operates via magnetostriction (similar to PFW/PZT) [12, 13]. Dilsom et. al [10 and 11] reported for room-temperature single phase multiferroic magnetoelectrics on $Pb(Fe,\ Ta)_x(Zr,Ti)_{(1-x)}O_3$ and $Pb(Fe,\ Nb)_x(Zr,Ti)_{(1-x)}O_3$ quaternary B-site perovskites, the Fe/W/Zr/Ti compounds exhibit only biquadratic coupling between polarization (P) and magnetization (M), and not linear magnetoelectricity [11 - 13]. Schiemer et. al. proved that PFT/PZT solid solutions shows the

room temperature multiferroic properties due to the magnetoelastic [14]. Because of these above reasons, it will limit device applications severely: Strain interactions are subsonic, and hence the device may be too slow for electronic gadget memory device. And the quadratic dependence upon H will necessitate a complex pulse sequence for rewrite operations [8 - 16]. Now one has to look for the material which exhibits multiferroic property not due to the strain induced.

In view of this, PFN and PFW are the outstanding candidates due to the origin of ME coupling in them is a d – orbital mechanism [1-6]. By making the solid solution of PFN and PFW (PFN_{1-x}-PFW_x), the effective T_N and T_C can be tuned to RT or near RT, leading to RT multiferroics.

Recently, the effect of addition of PFW (x=0.6) on the magnetic and electric properties of PFN_{1-x}-PFW_x ceramics have been reported [7]. However, a systematic investigation, with increasing x on the magnetoelectric properties of PFN_{1-x}-PFW_x multiferroics, has not yet been done. In this work, PFN, PFW and their solid solutions were synthesized through modified solid state reaction and detailed studies on their structural, magnetic and electric properties are investigated through XRD and ND, bulk magnetization (M-H loop), temperature dependent magnetization, Mössbauer spectroscopy and ferroelectric measurements. We hope that our work will be helpful in achieving a deeper understanding of the medications on structure, electric and magnetic properties in PFN_{1-x} - PFW_x and that such a material can be used in RT and near RT magnetoelectric multiferroic devices.

2. EXPERIMENTAL

2.1. Sample preparation technique

Polycrystalline samples of PFN_{1-x}-PFW_x (x = 0.0, 0.2, 0.4, 0.6, 0.8 and 1.0) were prepared by a modified solid state reaction method at a relatively low sintering temperature (<850 °C) and using high-purity (99.9%) ingredients; PbO (SD fine, India), Fe_2O_3, Nb_2O_5 (Sigma Aldrich) and WO_3 (SD fine, India). The detailed synthesis methods for the preparation of PFN and PFW are reported elsewhere [17, 18].

2.2. Characterization techniques

To check the phase formation of the polycrystalline samples, we used X-ray diffraction (XRD) technique employing a high-resolution X-ray diffractometer (Phillips 1070 model with CuK_α radiation (λ = 1.5406 Å). Fourier transform infrared (FTIR) spectroscopy is performed by using Bruker Tensor 27. Scanning Electron Microscopy (SEM) was used for studying the microstructure and morphology of the samples. The neutron powder diffraction (NPD) measurements were carried out at UGC-DAE CSR Mumbai Centre, Dhruva reactor, BARC Trombay India, using a PSD (Position Sensitive Device)– based focusing crystal diffractometer. The 5mm diameter sintered pellets were inserted in a vanadium can and used for the ND experiment. The neutron diffraction data was collected using a wavelength of 1.48 Å at RT (300 K) and in the 2θ range of 10° to 110°. The *Fullprof* suite programs [19] were used for Rietveld refinement of the ND data. Raman spectra were collected at RT using Ocean Optics ID Raman micro Raman spectrometer (Dunedin, USA) with a backscattering configuration and the excitation laser wavelength of 785 nm and with an output power of 70mW. Magnetization studies were carried out on a vibrating sample magnetometer (VSM) attached to a physical property measurement system (*Quantum Design* PPMS). Transmission Mössbauer spectrum was measured at RT by using a ^{57}Co source (Rh – matrix, ~15 mCi) mounted on a constant acceleration Mössbauer drive from SEE Co., USA and a proportional counter. For the least – squares fitting of the Mössbauer spectrum we used the computer program *NORMOS* written by R. A. Brand [20]. The electrical measurements, thinned

samples were used to make parallel plate capacitor geometry. The silver (Ag) paint used to make electrodes and after fired at 100 - 150 ºC for 30 minutes. The ferroelectric loop (P-E) tracer M/s Radiant Instruments, USA used for the measurement of RT ferroelectric (P-E) loop and during the measurements, pellets were immersed in silicon oil to prevent electric arcing, if any, at high applied voltages**.**

3. RESULTS AND DISCUSSION

3.1. XRD results: Structure and symmetry

Fig. 1(a - f) depicts the Rietveld refined XRD patterns of $PFN_{1-x} - PFW_x$ (x = 0.0, 0.2, 0.4, 0.6, 0.8 and 1.0) solid solutions at RT. It reveals the formation of single phase perovskite structure without any other secondary phases (e.g., pyrochlore). The diffraction patterns were indexed according to previously reported results, as monoclinic structure for PFN and cubic for PFW [21 - 24]. Achieving single phase is a difficult task especially in Pb based materials, due to the easily formation of unwanted impurity phases, like pyrochlores ($Pb_2Nb_2O_7$, $PbNb_2O_{6.5}$) along with the perovskite phase. The formation of pyrochlore phase is the major issue in Pb based system; it is due to the evaporation of Pb above 850 °C during the annealing. To compensate Pb deficiency in the high temperature processing, 10% excess PbO was added to each composition. In order to prevent the PbO loss and to maintain required stoichiometry, an equilibrium PbO vapor pressure was established with $PbZrO_3$ as setter by placing pellets in covered alumina crucibles.

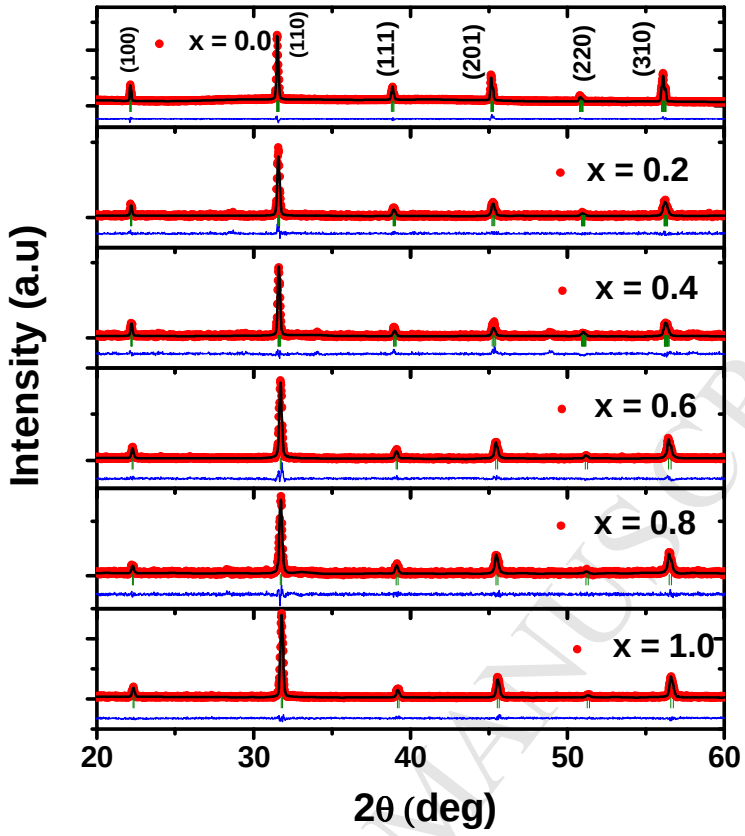

Figure1. Observed (red circle) and calculated (continuous black line) profiles of the X-ray powder diffraction for PFN, PFW and solid solutions. The lowest curve (blue line) shows the difference between experimental and calculated patterns. (a) x = 0.0, (b) x = 0.2 (c) x = 0.4 (d) x = 0.6 (e) x = 0.8 and (f) x = 1.0 is shown above. (a) x = 0.0, (b) x = 0.2 (c) x = 0.4 are the *monoclinic* structure with *Cm* space group and (d) x = 0.6 (e) x = 0.8 and (f) x = 1.0 are the *cubic* structure with *Pm*-3*m* space group.

Recently, we have reported [18, 25 - 27] the well-fitted refinement of XRD data for PFN and PFW which confirms the *monoclinic* (with *Cm* space group) and *cubic* (with *Pm*-3*m* space group) structure for PFN and PFW, respectively. The Rietveld refinement on XRD patterns of solid solutions of x = 0.2 to 0.8 were performed initially with *monoclinic* structure (*Cm*) for x = 0.2 and 0.4 and *cubic* structure (*Pm*-3*m*) for x = 0.6 and 0.8, which did not give perfect fitting. Later, we assumed both monoclinic and cubic phases co-existing with

different ratio for x = 0.2 to 0.8 solid solutions and which shows better fitting. The detailed structural studies are explained in next section.

FTIR spectra of solid solutions were recorded in the range of 400 – 1000 cm^{-1} and are shown in Fig. 2. The strong absorption bands were observed around 400 - 560 cm^{-1} for all the samples and these bands are attributed to the bending and stretching vibrations of metal - oxide bonds such as Pb – O, Fe – O, Nb – O and W - O [28]. On increasing x, there was significant shift of absorption peak around 500 $cm^{-1}$and also a significant change in its shape. This is due to the addition of W ion in between the O – Nb/Fe – O bonds. This feature confirms the perovskite structure. The morphological studies of solid solutions were carried out by scanning electron microscopy (SEM). The SEM micrographs of representative solid solutions with x = 0.0, 0.6 and 1.0 are shown in Fig. 3 (a), (b) and (c), respectively. From the micrographs, average grain size was found to be 2 µm for all the samples. In order to investigate the RT crystal structure of solid solutions accurately, we performed ND measurements and deduced the structural parameters using the standard Rietveld technique. The atomic positions, coordinates of different structures, space groups and structural parameters are summarized in Table I.

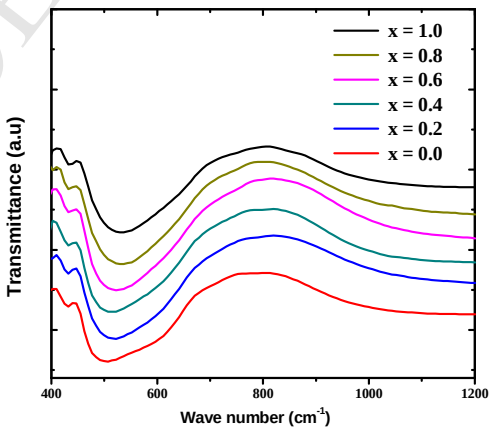

Figure 2. FTIR spectra of PFN, PFW and solid solutions.

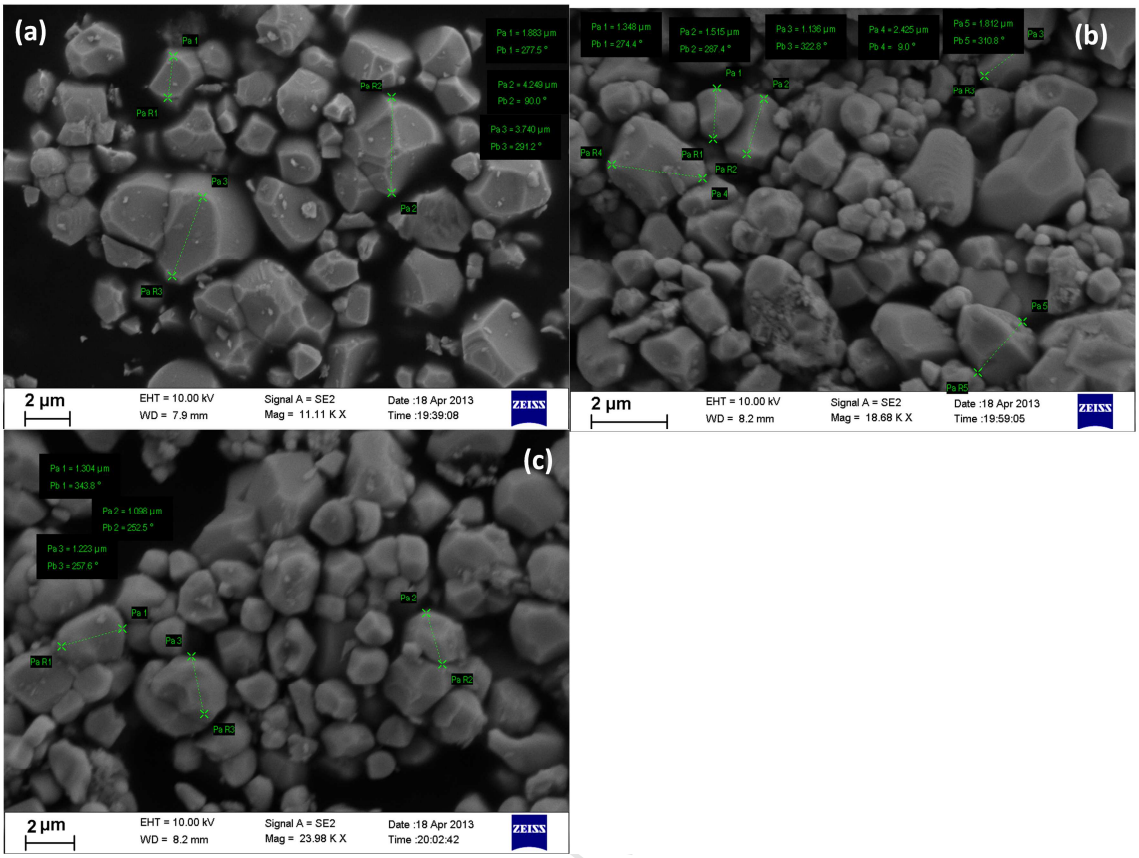

Figure 3. Scanning electron micrographs of solid solution with x = 0.0 (a), 0.6 (b) and 1.0 (c).

3.2 Neutron diffraction studies

RT and low temperature ND data for x = 0.0 are reported elsewhere [26] along with the structure and existing magnetoelectric coupling through the spin lattice coupling. The RT ND data were refined (nuclear structure) with the monoclinic structure with *Cm* symmetry. Figure 4 (a) shows the Rietveld refined data for all the solid solutions with the reasonable fitting between the calculated and experimental data. The obtained lattice parameters are reported elsewhere [26] and are in excellent agreement with literature reports [29]. There are four atoms in the asymmetric unit with Fe/Nb, Pb, O_1 and O_2, in this Fe, Nb and O_1 in (1b) sites at (x, y, z), Pb (1a) sites at (0, 0, 0) and O_2 in (2c) at (x, 0, z) in the monoclinic phase with *Cm* space group. Figure 5(a) shows the polyhedral view of the monoclinic structure at x = 0.0 RT.

In order to confirm the co-existence of monoclinic and cubic phases, as observed from the XRD studies, Rietveld refinement was performed on RT ND data for x = 0.2 to 0.8. It is confirmed that the data could be well refined with co-existence of two phases with different ratios compared to respective single phase refinement. Initially, we assumed monoclinic phase as dominant phase and cubic phase as minor phase for x = 0.2. The refinement results shows that percentage of phase composition is 98.37(0.4)% for monoclinic phase and 1.63(0.4)% for cubic phase. Similarly, for x = 0.4 monoclinic phase is 61.48 (0.7)% and cubic phase is 38.52 (0.6)%, for x = 0.6 monoclinic phase is 12.25 (0.2)% and cubic phase is 87.75 (0.2)%, for x = 0.8 monoclinic phase is 7.88 (0.5)% and cubic phase is 92.12 (0.9)%, respectively. Fig. 4 (b to e) shows the Rietveld refined ND data for x = 0.2 to 0.8. In Fig. 4 the highlighted region shows emergence of new peak (around $2\theta \sim 18.51°$), corresponding to magnetic ordering, for x = 0.6, and the intensity of peak increases with increasing x (x = 0.8 and 1.0). It shows the evolution of G-type anti-ferromagnetic ordering with T_N (magnetic phase transition from paramagnetic to G-type antiferromagnetic structure) at or above RT for the compositions above 0.6. The observed magnetic reflections are (100), which can be indexed by using the propagation vector k = [½ ½ ½] [29, 30 and 31].

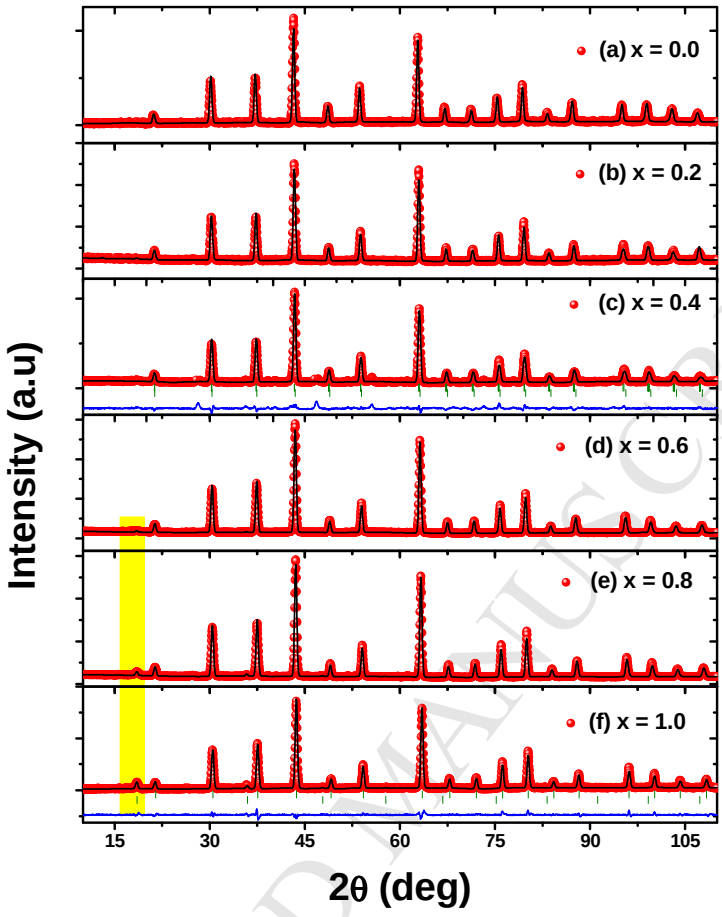

Figure 4. Room temperature NPD patterns for (a) x = 0.0, (b) x = 0.2 (c) x = 0.4 (d) x = 0.6 (e) x = 0.8 and (f) x = 1.0 measured on FCD using λ = 1.48 Å. The Rietveld analysis of the ND data is also shown in the figure. In the panel (d), (e) and (f), the magnetic peaks are seen around 18.4°, 35.7° and 48.0°. In this figure, the first row of vertical lines indicates the nuclear structure, the second row corresponds to the AFM phase (k = ½ ½ ½).

Figure 4 (f) shows the refined RT ND data for PFW with the evident of reasonable fitting between the calculated and experimental data. The RT ND data and structural parameters were reported elsewhere [18, 27]. The RT Rietveld refinement were performed on ND data, shows the *cubic* or pseudo cubic structure with *Pm*-3*m* symmetry. The atoms were fixed at their special positions, for Pb (1a), for Fe/W (1b) and (3c) for O, respectively. The model for

the *cubic* phase is typically observed in simple perovskites, where, the two B - cations were located at the same crystallographic 1b Wyckoff sites (½ ½ ½), Pb atoms at 1a sites (000) and O atoms at the 3c sites (½½ 0). In the octahedral Fe and W cations were distributed. The obtained lattice parameters are reported elsewhere [18, 27] and shows excellent agreement with other reported results [7, 18]. A polyhedral view of the cubic structure of PFW is shown in Fig. 5(b) and Fig. 5 (c) show the obtained G-type antiferromagnetic structure at RT.

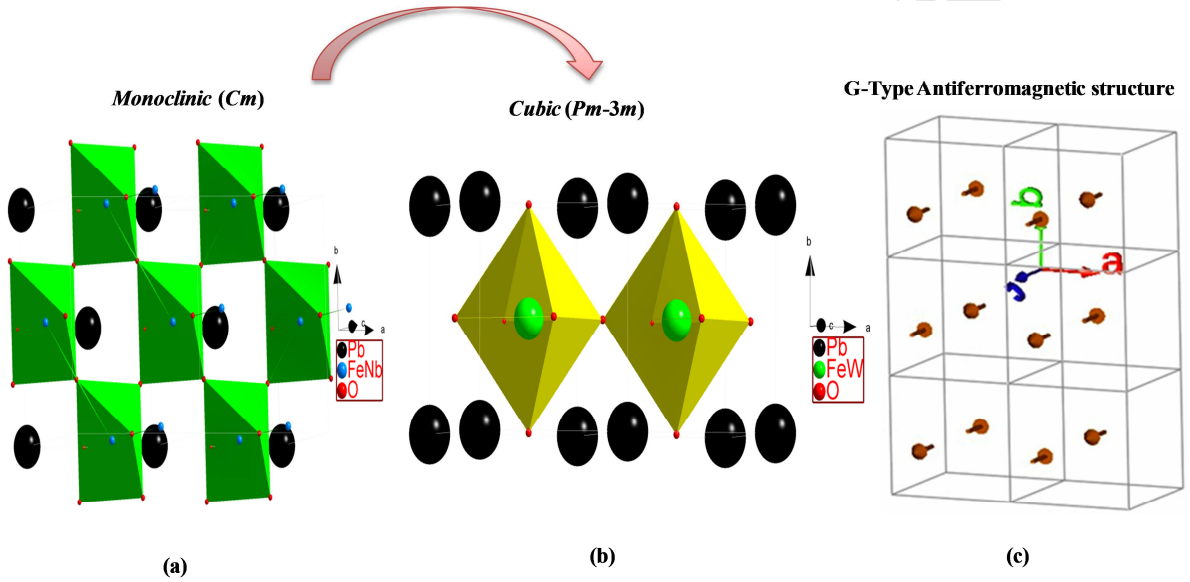

Figure 5. (a) A polyhedral view of the monoclinic perovskite structure of $Pb(Fe_{0.5}Nb_{0.5})O_3$ (x = 0.0) at room temperature. (b) A polyhedral view of the cubic perovskite structure of $Pb(Fe_{0.67}W_{0.33})O_3$ (x = 1.0) at room temperature and (c) G-type antiferromagnetic structure at RT for PFW.

3.3 Phase transition from monoclinic (*Cm*) to cubic (*Pm-3m*)

The PFN and PFW solid solutions are the promising candidates for the RT or near RT magnetoelectric multiferroics. From the results of magnetic and ferroelectric properties, the x = 0.2, 0.4 and 0.6 solid solutions shows near RT magnetoelectric multiferroics properties compared to other solid solutions (0.8 and 1.0).

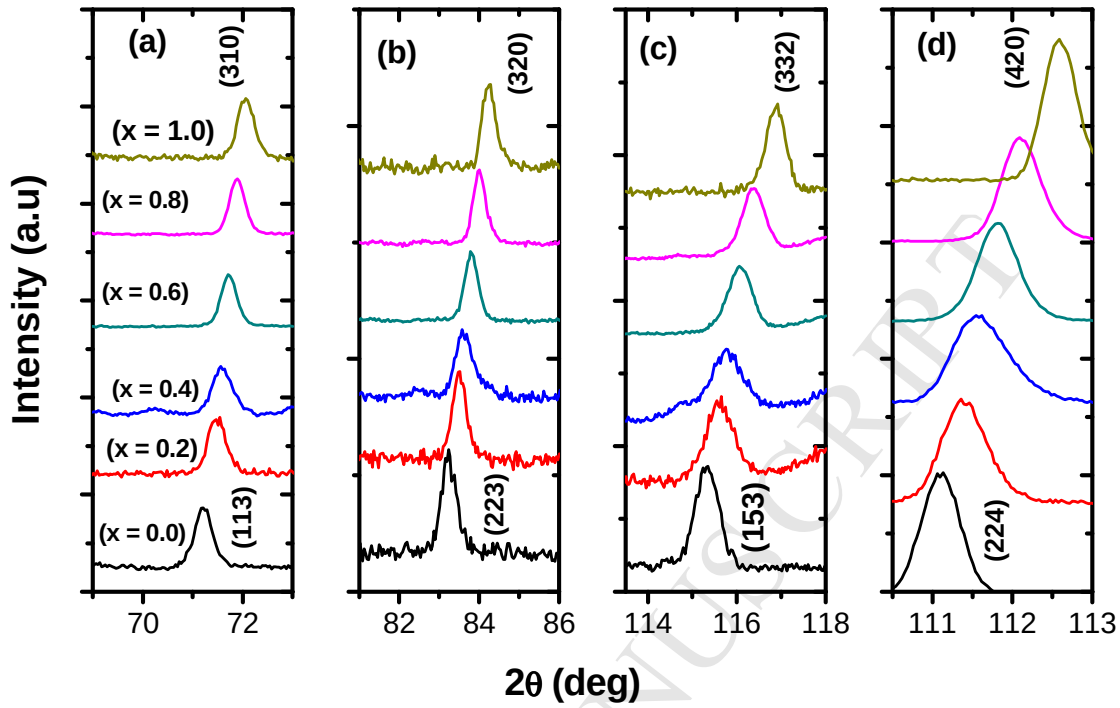

Figure 6. Zoomed ND raw data of PFN, PFW and its solid solutions at selected 2θ range showing nuclear structure peaks with different (hkl) indices.

In order to understand the evolution of (113), (223), (153) and (224) nuclear peaks the RT ND raw data of PFN_{1-x} – PFW_x (x = 0.0, 0.2, 0.4, 0.6, 0.8 and 1) is shown in Fig. 6 (a, b, c and d) in the range $69° \leq 2\theta \leq 113°$. With the increase of x there is a systematic shift in the peak positions toward the higher diffraction angle (2θ) that could be due to the phase transition and substitution of ions with different ionic radii at B-site. In this case Fe^{3+} (0.67 Å), Nb^{5+} (0.64 Å) and W^{5+} (0.62 Å) are the different ionic radii. With the increase of x, the peaks associated with monoclinic phase (113), (223), (153) and (224) reflections show systematic evolution towards cubic phase (310), (320), (332) and (420) in accordance with the evidences of (a) anomalous broadening and asymmetry in peaks, (b) peak shift and (c) increase of peak intensity and reduction in peak splitting were observed. It can be observed that as the value of x increases, the cubic phase starts to appear. This confirms an evidence of

existing phase transition from monoclinic to cubic. The coexistence of monoclinic and cubic phase i.e. the Morphotropic Phase Boundary (MPB) is expected at x = 0.6 composition for $PFN_{1-x} – PFW_x$ solid solution. The above observed features in (a), (b), (c) and (d) are similar to those of earlier reports in (1-x) $[Pb(Fe_{1/2}Nb_{1/2})O_3] – x\ CaTiO_3$, (1-x) $[Pb(Mg_{1/3}Nb_{2/3})O_3] – x\ PbTiO_3$, (0.85 - x) $Pb(Mg_{1/3}Nb_{2/3})O_3$ -0.10$Pb(Fe_{1/2}Nb_{1/2})O_3$ - 0.05$PbZrO_3 – x\ PbTiO_3$ and 0.75 $Pb(Fe_{2/3}W_{1/3})O_3$–0.25$PbTiO_3$ [32 – 35].

Table 1: Structural parameters, symmetries, phase fraction, magnetic moment and integrated intensity of magnetic peak (I) of RT ND data refinement for x = 0.0, 0.2, 0.4, 0.6, 0.8 and 1.0 solid solutions.

Parameters	**0.0**	**0.2**		**0.4**		**0.6**		**0.8**		**1.0**
Symmetry	*Cm*	*Cm*	*Pm-3m*	*Cm*	*Pm-3m*	*Cm*	*Pm-3m*	*Cm*	*Pm-3m*	*Pm-3m*
a (Å)	5.6801(4)	5.6665(2)	3.9943(6)	5.6605(1)	3.9947(3)	5.6656(1)	3.9957(1)	5.6539(4)	3.9982(1)	3.9776(3)
b (Å)	5.6724(3)	5.6569(2)	3.9943(6)	5.6623(2)	3.9947(3)	5.6182(1)	3.9957(1)	5.6094(1)	3.9982(1)	3.9776(3)
c (Å)	4.0273(3)	4.0122(1)	3.9943(6)	4.0092(1)	3.9947(3)	4.0030(2)	3.9957(1)	4.0016(1)	3.9982(1)	3.9776(3)
Phase (%)	100	98.37(0.4)	1.63(0.4)	61.48(0.7)	38.52(0.6)	12.25(0.2)	87.75(0.2)	7.88(0.5)	92.12(0.9)	100
B(°)	89.82(1)	89.94 (1)	90	89.965(6)	90	90.624(1)	90	90.544(4)	90	90
Magnetic structure with Propagation vector: k = [½ ½ ½]										
Magnetic moments										
μ_{AFM}	0.000	0.000		0.000		0.674		0.886		1.008
Magnetic R factor										
R Mag	0.00	0.00		0.00		28.9		14.8		22.6
Integrated Intensity of magnetic peak	0.00	0.00		0.00		461.53		621.22		839.20

The existing phase transition furthermore evidenced from the two phase refinement of solid solutions. The Rietveld refinements were carried out on PFN, PFW and solid solutions by considering above parameters such as *monoclinic* (*Cm*), *cubic* (*Pm-3m*) and *monoclinic* (*Cm*) + *cubic* (*Pm-3m*) phases. Initially, we performed Rietveld refinement by assuming single phase with *Cm* symmetry for x = 0.2 composition. The same x = 0.2, refined by considering initial stoichiometric ratio of 80% *Cm* and 20% *Pm*-3*m* symmetry show best fitting with reasonable R factors in two phase refinement. The refinement results for x = 0.2

shows 98.37 (0.45) % *Cm* symmetry and 1.63 (0.01) % *Pm*-3*m* symmetry. Then later on, the same method was adopted for the refinement of all the other solid solutions. It is observed that with the increase of x in $PFN_{1-x} – PFW_x$, the % of *Cm* symmetry decreased and *Pm-3m* symmetry dominated. The results of existing phases with different x are tabulated in Table I. This structural phase transition from monoclinic (*Cm*) to cubic (*Pm*-3*m*) symmetry from PFN to PFW, is well corroborated with Raman studies (discussed in next section).

As expected, the ND patterns of x = 0.2 and 0.4 shows only nuclear (chemical) structure, whereas x = 0.6 and 0.8 exhibits both magnetic and nuclear structure at RT. As mentioned in introduction, PFN and PFW show multiferroic properties below RT because either their T_c or T_N is below RT (T_C ~ 380 K and T_N ~ 155 K for PFN; T_C ~ 150 K and T_N ~ 385 K for PFW). The solid solution of PFN_{1-x} - PFW_x (x = 0.0, 0.2, 0.4, 0.6, 0.8 and 1.0) is explored here to achieve near RT multiferroic properties by tuning both T_c and T_N to RT or above. Figure 4 clearly shows the origin of new peak (magnetic) around 18.51° with x=0.6 and above in $PFN_{1-x} – PFW_x$. The intensity of the peak gradually increases with x = 0.6 onwards. This is a clear evidence of magnetic transition from paramagnetic to antiferromagnetic occurring at or above RT for x = 0.6 onwards. The possible magnetic structure compatible with the symmetry have been determined with the aid of the representation analysis technique described by Bertaut [36] by using the program BasIreps contained in the FULLPROF Suite package [30]. The originated magnetic peak in both solid solutions could be indexed using G-type AFM structure with the propagation vector k = (½ ½ ½).

3.4 Raman spectroscopy

Raman scattering spectroscopy is an effective tool to study the local structure of materials. The room-temperature Raman spectra of PFN_{1-x} - PFW_x (x = 0.0, 0.2, 0.4, 0.6, 0.8 and 1.0) solid solutions are shown in Fig. 7 (a - f). The Raman spectrum of PFN contains a

series of broad overlapping bands, which is typical of samples with monoclinic phase [37]. According to the factor group analysis the monoclinic PFN has 10 Raman modes of symmetry that are 242.7, 281.1, 343.3, 402.8, 431.7, 486.6, 574.2, 695.5, 780.0, and 858.2 cm^{-1}, respectively, which can be ascribed to the A1g, Eg, F1g, 4F1u, 2F2g and F2u optical phonon modes for a simplified cubic perovskite ABO_3 lattice in three dimensions with two types of cations at B-position [38]. Among these pure Raman active four modes are the A1g, Eg and 2F2g phonons, and the rest become visible in Raman spectra due to local structural distortions with respect to the ideal lattice. The approximate assignment of the modes in the Fig. 7 (a), made according to previous studies of $PbFe_{0.5}Nb_{0.5}O_3$ at ambient pressure [39, 40], and also Pb-based relaxor oxides [41-44]. The analysis was done on the basis of previous reports on pure PFN and similar Pb based systems [45].

The modes, located in the region 700 – 850 cm^{-1} correspond to symmetric and asymmetric stretching vibrations of oxygen octahedra around Fe/Nb atoms of Nb – O – Nb (A1g – 780.0 cm^{-1}), Nb–O (Eg – 858.2 cm^{-1}), and Nb – O – Nb (F1u – 695.5 cm^{-1}) symmetry corresponds to monoclinic phase. The region of 400 – 530 cm^{-1} corresponds to the bending O - Fe/Nb - O vibrations of F2g (574.2 cm^{-1}) and F1u (486.6 and 431.7 cm^{-1}) symmetry.

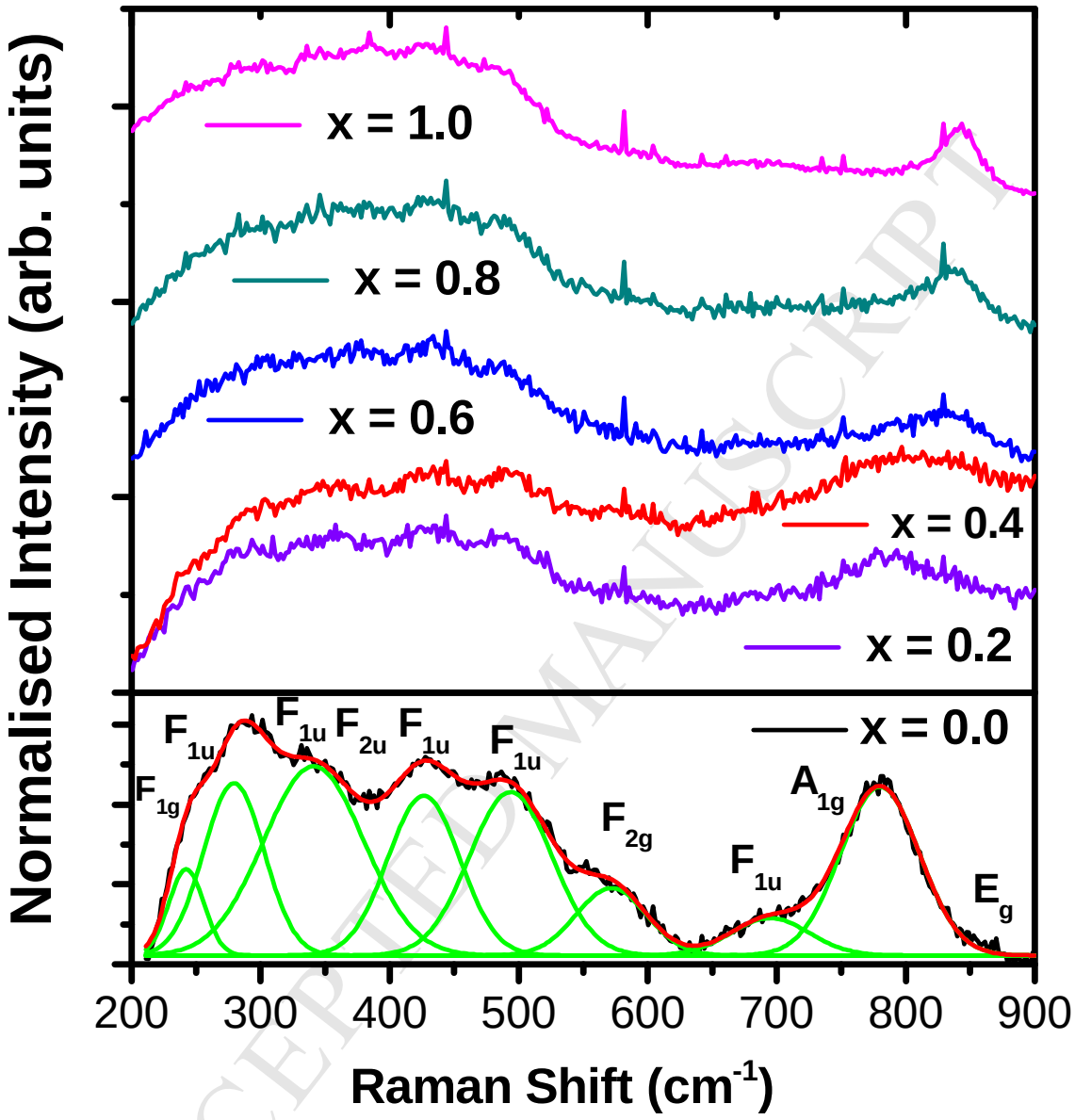

Figure 7. RT Raman studies on (a) x = 0.0, (b) x = 0.2 (c) x = 0.4 (d) x = 0.6 (e) x = 0.8 and (f) x = 1.0.

The modes at the region of 200–400 cm^{-1} are related to Pb - O bond stretching vibrations of F2u symmetry (402.8 cm^{-1}), Fe/Nb-cation localized mode of F1u symmetry (281.1 cm^{-1}), and the rotational mode of Fe/Nb-O_6 octahedra of F1g symmetry (242.7 cm^{-1}).

Figure 7 shows that room temperature Raman spectra of PFN and it is well matching with the reported Pb based relaxors [40-42] and where the broad peak at 780 to 791 cm^{-1} is well distinguished from the other modes. The modes located in the region 700 – 850 cm^{-1} correspond to stretching vibrations of oxygen octahedra around Fe/Nb atoms or Nb – O – Fe (stretching mode) of A_{1g} (790 – 800 cm^{-1}), E_g (849.3 cm^{-1}), and F_{1u} (690 - 700 cm^{-1}) symmetry in correlation with the $Pb(Mg_{1/3}Nb_{2/3})O_3$, Nb – O – Mg stretching mode [43, 44], being a characteristic peak in the Pb – based complex perovskite structure relaxors. The broad region of Raman shift 400 – 530 cm^{-1} involves the bending O – Fe and Nb - O vibrations of F_{2g} (558.0 cm^{-1}) and F_{1u} (473.6, 429.2 cm^{-1}) symmetry.

From the refinement of ND data found that, Pb (Lead) is never in its ideal Wyckoff position [45, 46] and also, the B site cations (Fe^{3+} and Nb^{5+}) local ordering within a disordered matrix [47] and it is well supported by the Garcia –Flores et al. [39] report. The presence of Fe^{3+} cations in the octahedral B site, possible indirect magnetic nature of these modes can be considered since PFN presents, in addition to ferroelectric and magnetic properties, which is responsible for the peak at 791 cm^{-1}. Indeed, this magnetic ordering is cause of spontaneous magnetostriction, through the atomic displacements.

As can be clearly seen in Fig. 7 (b - e), the general aspects of the Raman spectra show a marked change with the increase of x in PFN_{1-x} - PFW_x. It indicates that a continuous change in symmetry (i.e. monoclinic–pseudocubic–cubic phase) [47, 48]. The observed changes clearly indicate a change at the octahedral site [38, 48, 49]. The main mode at ~780 to 835 cm^{-1} is shifted by varying x from 0.2 to 0.8, which is due to the Nb – W – O – W – Fe

stretching mode and it is a characteristic peak of Pb-based complex perovskite series. Also, the stretching modes of Nb – W – O – W – Nb (F1u – 695.5 cm^{-1}) were disappeared on increasing x. Hence, it confirms the conversion of non-centrosymmetric to centrosymmetric phase. The region around 400 to 530 (486, 431, 402) and 281, 242 cm^{-1} stretching modes were disappeared on x = 0.6 and onwards. Hence, this is the evidence of existing centrosymmetric cubic (*Pm*-3*m*) phase. At x = 0.2 to 0.8 solid-solutions has both monoclinic (*Cm*) and cubic (*Pm*-3*m*) features.

Figure 7 (f) depicts the Raman spectra of x = 1.0 and observed an broad intense A – mode at 850 cm^{-1} which is the stretching mode of Fe^{+3} – O – W^{+6} bonds corresponds to the cubic structure with *Pm*-3*m* space group. Around 380 – 432 cm^{-1}, well-pronounced broad peak near the BO_6 octahedral B - mode, indicates the stretching between Fe^{+3} – O – Fe^{+3} and W^{+6} – O – W^{+6} [50, 51]. The near 268 cm^{-1} is B-mode band and related to the localized B-cations. The phonon modes are related to the oxygen-localized BO_6 rotational mode might contribute to the band near 200 – 298 cm^{-1}. The band around 700 cm^{-1} clearly indicates the evidence of antisymmetrical BO_6 bending or translation modes in which phonon modes are oxygen-localized. The x = 0.2 and 0.4 shows similar behaviour of PFN, the shift is very small and x = 0.6 and 0.8 shows the similar behaviour of PFW. It is more evidenced from the highlighted region and tick mark show in Fig. 7 (a) – (f) for changing the symmetry and phase transition from monoclinic to cubic.

3.5 Magnetic properties

The magnetic hysteresis loops of PFN_{1-x} – PFW_x for x = 0.0, 0.2, 0.4, 0.6, 0.8 and 1.0 solid solutions as shown in the Fig. 8. Slim hysteresis loops were found for x = 0.0, 0.2, 0.4 and 0.6 solid solutions, however the clear appreciable hysteresis loops were observed for x = 0.8 and 1.0. An improvement in coercive field and saturation magnetisation were observed with

increase in x. From the above results, it is clearly confirmed that the x = 0.0 and 1.0 exhibits the weak ferromagnetic ordering with small opening of loops [52] at RT with paramagnetic and antiferromagnetic phases, respectively [18]. The occurrence of weak ferromagnetic ordering is due to the disordered antiferromagnetic interactions through – Fe^{3+} – O – Fe^{3+} – superexchange paths and – Fe^{3+}– O – W – O – Fe^{3+} – super – super – exchange paths in the present samples [53]. However, from the magnetization curves, it is evident that the sample is not a conventional antiferromagnet. In fact, it is quite probable that the Fe^{3+} - rich islands present uncompensated magnetic moments, resulting in a weak - ferromagnetic (WFM) behavior, which gives rise to a net magnetization in each island, manifested as a macroscopic magnetization of the solid solutions [54]. Fig. 8 inset shows the enlarged view of M-H loops near origin showing clear coercive field, which is increases with x.

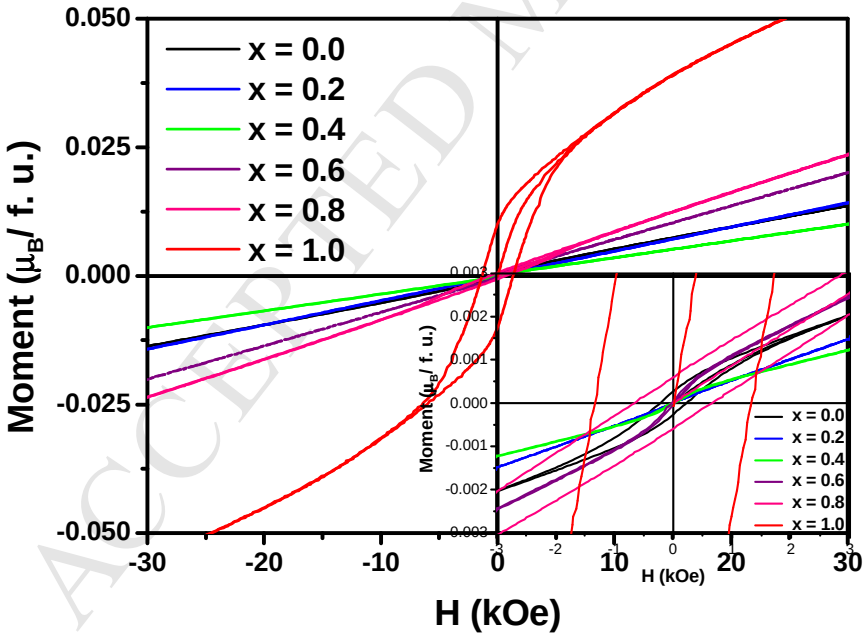

Figure 8. Magnetization hysteresis (M–H) loops of (a) x = 0.0, (b) x = 0.2 (c) x = 0.4 (d) x = 0.6 (e) x = 0.8 and (f) x = 1.0.

From the XRD and ND data, it is confirmed that there is no evidence of coexistence of Fe_2O_3 - related phases (secondary phases) with the perovskite structure. This confirms that the observed magnetic responses must be associated to the perovskite PFN and PFW pure phases. The x = 1.0 pure PFW is known [7, 18] to exhibit antiferromagnetic behaviour above the RT and it is clearly evidenced from the observed M-H loop results (with well saturated remanence and coercive field).

Figs. 9 (a - f) depict the results of magnetization as a function of temperature (M(T)) measurements, with maximum applied field of 500 Oe, for all the solid solutions in zero-field cooled (ZFC) and field cooled (FC) modes. From the M(T) measurements, it is observed that, the Néel transition temperature (T_N) of both PFN and PFW is around 155 K and 350 K, respectively and it is well matched with the earlier reports [17, 18, 25 – 27, 29, 39]. In fact, two types of magnetic ordering have been observed from the temperature dependence of magnetization (Fig. 9 (a to f)), which arise from different magnetic interactions: a strong superexchange interaction between the Fe^{3+} – O – Fe^{3+} at T_{N1} ~ 155 K (for x = 0.0), this interaction cause by the origin of a G-type antiferromagnetic structure. The another weak superexchange interaction between the Fe^{3+} – O – W – O – Fe^{3+} , caused by local short range order in the B site, which is responsible for the anomaly around T_{N2} ~ 20 K (for x = 0.0). The low temperature magnetic ordering occur in the range of T_{N2} ~ 20 K, while the high temperature ordering, referred to antiferromagnetic to paramagnetic transition at T_{N1} ~ 155, 194, 288, 295, 310 and 350 K for x =0.0, 0.2, 0.4, 0.6, 0.8 and 1.0, respectively. Intriguingly, on increasing x, the Néel temperature (T_N) shifted drastically from 155 K to 194, 288, 295, 310 and 350 K, respectively. The anomaly at below 20 K in the ZFC (M-T) curve is known to be spin glass freezing (T_g) behaviour [17] in all the samples. The Fig. 10 shows the systematic shift of T_N towards RT (155 – 350 K). The observed shift increases with increasing x. This shift of T_N corroborates with the tuning of T_N in PFN and PFW solid

solutions and it is comparable with recent report on Pb(Fe, M)$_x$ (Zr,Ti)$_{(1-x)}$O$_3$ [M = Ta, Nb] [11].

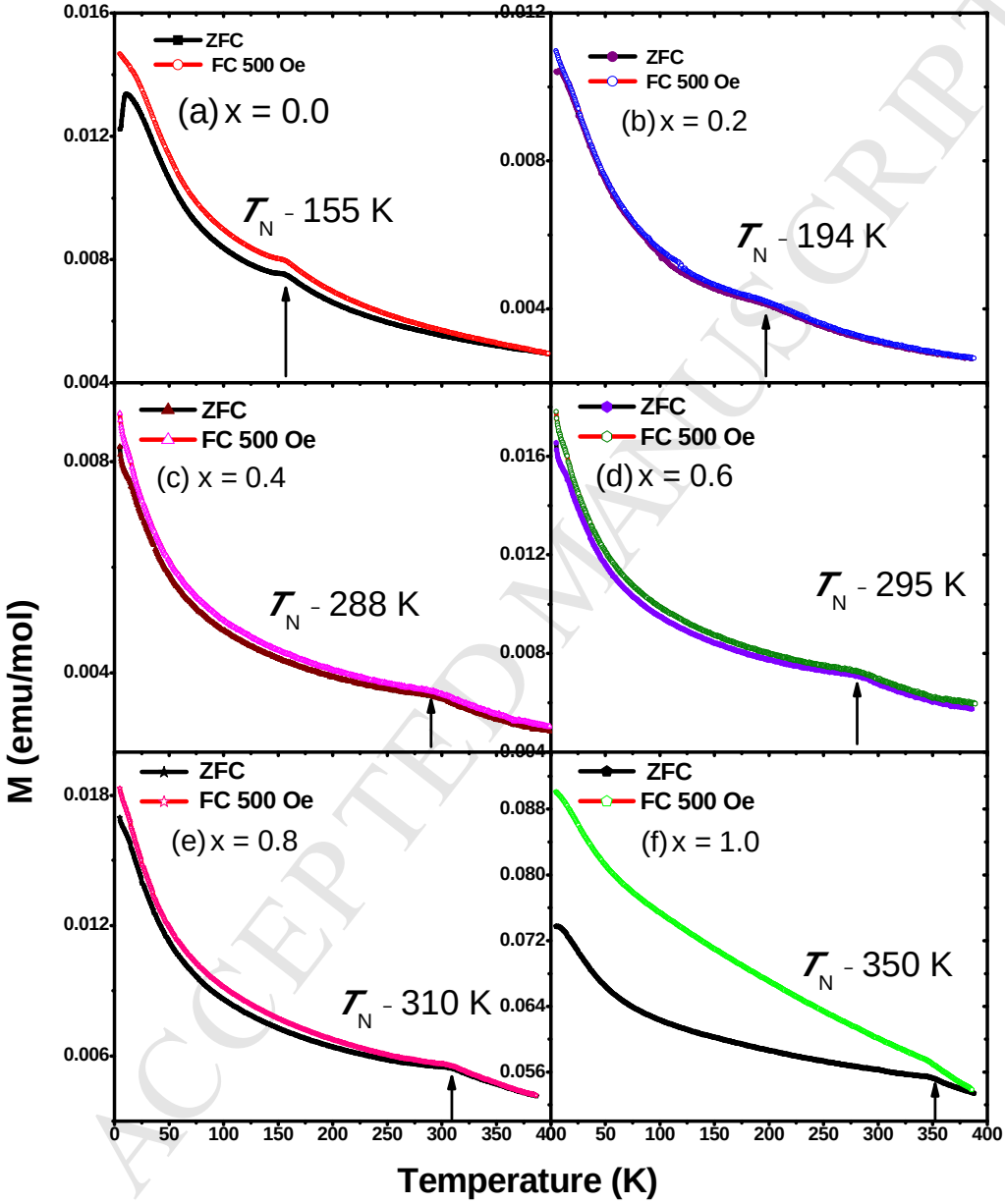

Figure 9. ZFC and FC curves for (a) x = 0.0, (b) x = 0.2 (c) x = 0.4 (d) x = 0.6 (e) x = 0.8 and (f) x = 1.0.

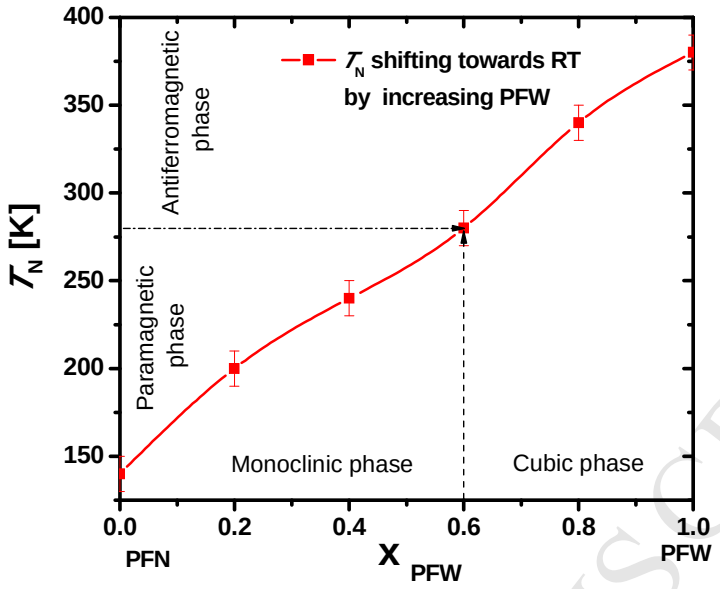

Figure 10. The dependence of T_N at different solid solutions of x = 0.0, 0.2, 0.4, 0.6, 0.8 and 1.0.

3.6 Mössbauer spectroscopy

Mössbauer spectral studies also reveal different magnetic ordering. The Mössbauer spectra for x = 0.0, 0.2, 0.4, 0.6, 0.8 and 1.0 are shown in Fig. 11 (a to f). The extracted Mössbauer parameters are listed in Table II. The RT Mössbauer studies for x = 0.0 and 1.0 are reported elsewhere [9 and 43] and are well matching with the other reports [5, 52, 55, 56]. The spectra shows the magnetic signature which corresponds to disordered Fe^{3+} ions in *Cm* symmetry for x = 0.0 and *Pm*-3*m* symmetry for x = 1.0 and with two different crystallographic environments for x = 0.2, 0.4, 0.6 and 0.8. Fig. 11 (a) shows the x = 0.0 Mössbauer spectrum confirmed no magnetically splitted doublet at RT implying that there are no significant internal magnetic field of the sample (due to the T_N ~ 155K) [26, 50, 51]. The x = 0.0 is fitted by a single quadrupole doublet and existing doublet is due to the Fe^{3+} ions in an octahedral environment. The non-zero electric quadrupole splitting demonstrates that the Fe

and Nb ions occupy non-cubic off-center sites and are randomly disordered around the B sites of the perovskite octahedra.

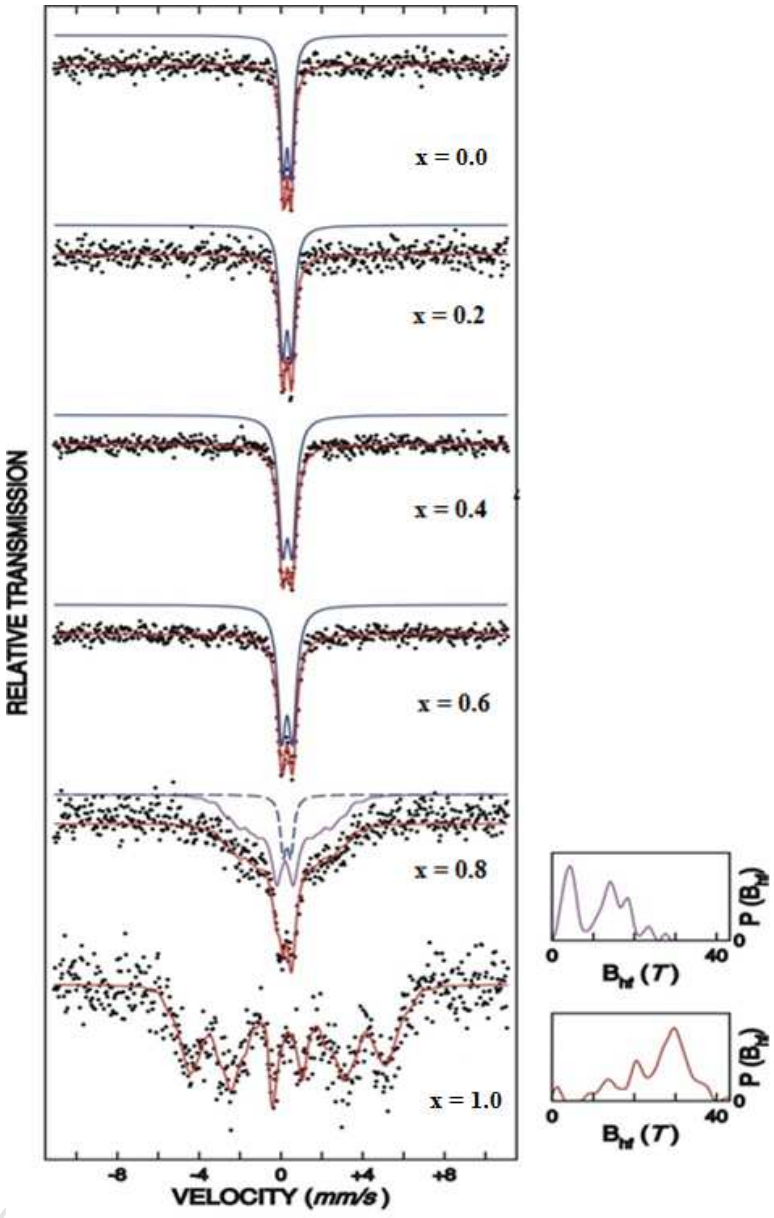

Figure 11. RT Mössbauer measurements on (a) x = 0.0, (b) x = 0.2 (c) x = 0.4 (d) x = 0.6 (e) x = 0.8 and (f) x = 1.0.

The Mössbauer spectra of x = 0.2, 0.4, 0.6 and 0.8 shows increased magnetic ordering with increasing x. It is expected that x = 0.0, 0.2 and 0.4 are paramagnetic in nature at RT and it is well reflected through the doublets, which is also in accordance with the earlier report on

x = 0.0 [52]. The x = 0.2, 0.4 and 0.6 are fitted by a single quadrupole doublet and x = 0.8 was fitted with two quadrupole doublet. Though ND, M-H loop and M(T) results show the origin of magnetic ordering at RT for x = 0.6, but Mössbauer results does not show any sextet features. It may be due to the highly ordered paramagnetic phase along with existing weak AFM magnetic ordering and x = 0.8 shows the origin of sextet, due to the increased magnetic ordering. But the width of the doublet is increased compared to x = 0.2 and 0.4. The observed isomer shift is decreased with increasing x. The isomer shift depends on s-electron density at the nucleus. If the density of s electron is small then isomer shift will be small and corresponding oxidation states naturally be large. This suggests that, with the increase in x the conversion of Fe^{+2} to Fe^{+3} becomes more prominent. Also hopping of electrons among Fe^{+2} to Fe^{+3} states is responsible for conduction and ferroelectric losses in the samples and it is well supported from the ferroelectric loops (discussed in next section).

The Mössbauer spectrum of the x = 1.0 at RT (Fig. 11 (f)) was fitted with a distribution of magnetic hyperfine fields, $P(B_{hf})$. The hyperfine field distribution is shown in the right hand side of Fig. 11 (f). The obtained average isomer shift (IS), quadruple splitting (QS), corresponds to the Fe^{3+} ions in an octahedral environment [55]. The average magnetic hyperfine field is ~ 25.5 ± 1.0 T. The broad hyperfine field distribution, $P(B_{hf})$, indicate that the environments of the Fe-ions are not the same, i.e., perfect compositional ordering is not achieved in the studied sample.

$P(B_{hf})$ for x = 0.8 and 1.0 is very similar to that of the earlier report by Raevskii et al. [55], where they fit the spectrum with a superposition of two sextets and a central (paramagnetic) doublet. From the $P(B_{hf})$ of x = 0.8 and 1.0, it is also clear that, along with the broad magnetic hyperfine field distribution, there exists a paramagnetic part, Fig. 10 (f)). Previously, Venevtsev et al. [56] reported a similar spectrum consisting of two sextets

observed after firing the x = 0.0 ceramics in oxygen, while the spectrum consists of a single sextet for a sample fired in air. The existence of a single sextet was due to fully disordered arrangement of Fe^{3+} ions, while the two sextets in a Mössbauer spectrum for x = 1.0 was associated with a partial disordering of Fe^{3+} and W^{6+} ions. The formation of two magnetic subsystems might be due to non- equivalent surrounding of iron ions in partially ordered and disordered regions. We too believe that, there is partial disordering in all our samples, which gives rise to the broad hyperfine field distribution, $P(B_{hf})$, particularly x = 0.8 and 1.0. The observed results confirm that there are regions where the Fe atoms are compositionally disordered. These results well supports to the ND, *M-H* loops and M(T) results.

Table 2. Hyperfine parameters obtained from Mössbauer spectra; ΔE_Q-quadrupole splitting, δ-isomer shift, Γ – line width, B_{hf} -magnetic hyperfine field.

Sample	Subspectrum	ΔE_Q (mm s^{-1})	δ (mm s^{-1})	Γ (mm s^{-1})	B_{hf} (T)
0.0	Doublet	0.3754	0.3040	0.3380	0.0
0. 2	Doublet	0.4355	0.3015	0.3916	0.0
0.4	Doublet	0.4666	0.3165	0.4856	0.0
0.6	Doublet	0.5273	0.3004	0.4884	0.0
0.8	Sextet	0.4450	0.2030	0.5029	13.54
1.0	Sextet	0.4299	0.6387	0.5228	25.24

3.7 Ferroelectric loops studies

The electric field induced polarization switching (P-E) behavior was studied at low frequency (20 Hz) utilizing Sawyer-Tower experimental set up. The RT electrical hysteresis loops for x = 0.0, 0.2, 0.4, 0.6, 0.8 and 1.0 solid solutions are shown in Fig. 12 (a - f). The ferroelectric loops exhibit leaky behaviour. This is due to the presence of mixed valence for Fe (Fe^{+2} and Fe^{+3}) which makes the sample conducting through hopping of electrons from Fe^{+2} to Fe^{+3}. The mixed valence of Fe is proved from the Mössbauer results. The existence of

ferroelectricity for PFN rich samples (x=0.0 and 0.2) in PFN_{1-x} – PFW_x solid solutions is evidenced through nearly saturated polarization curves, which show the RT ferroelectric nature (T_C ~ 385 K for PFN).

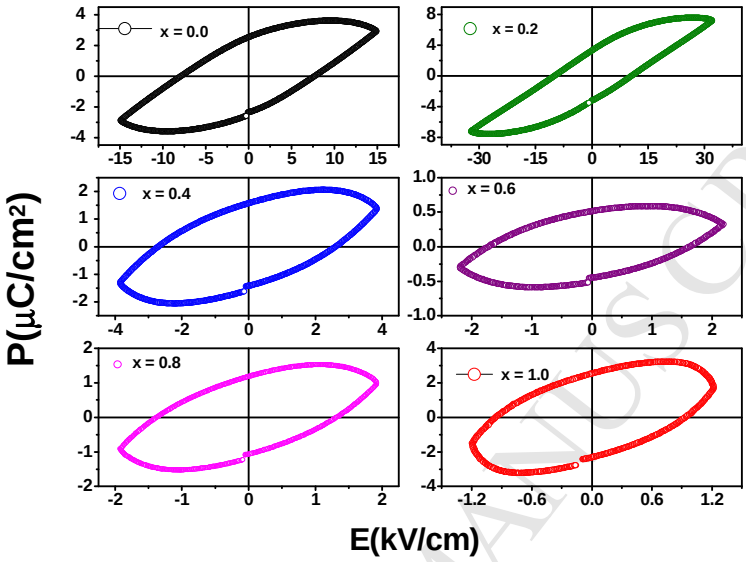

Figure 12. Polarization hysteresis (P–E) loops of (a) x = 0.0, (b) x = 0.2 (c) x = 0.4 (d) x = 0.6 (e) x = 0.8 and (f) x = 1.0.

Though, this P versus E loop is suggestive of the ferroelectric nature, however complete saturation of the polarization is not achieved at higher electric fields compare with recent reports on PFN, PFT, PFW and PZT solid solutions [8 - 16]. This may be due to the higher conductivity associated with the samples. However, with increase in x, the ferroelectric loops become more broad and leaky as the Fe content at the B site of the sample increase from 50% for x = 0.0 to 67% for x = 1.0). Importantly, the ferroelectric T_C, for x = 0.0 is around 350 K, after the solid solution with PFW, at x = 0.2 the T_C is expected to decrease from 350 K to 300 - 325K. Improved ferroelectric properties may be due to the reduction of oxygen vacancies. In case of x = 0.4 and 0.6 also, we expected similar behaviour in PE loops, but we did not see as expected due to the T_C being shifted to below RT. Unfortunately all our measurements are

done at RT. However, further low temperature measurements are required to understand the ferroelectric mechanism.

This indicates that the PFW can dilute the ferroelectric properties of the solid solutions by incorporating in to the ferroelectric matrix. The other reason for the leaky behaviour in the samples may be due to the presence of oxygen vacancies along with mixed valance states of *B*-site cations, which is likely to exist in ABO_3 type perovskite ferroelectric materials [18, 57].

4. Conclusion

In summary, PFN_{1-x} PFW_x single-phase solid solutions are successfully synthesized by solid-state reaction route (single step and columbite method). The structural, microstructural, phase transition, magnetic and ferroelectric properties of solid solutions are investigated. The results of ND and Raman scattering spectra show PFN_{1-x}-PFW_x solid solutions undergo a structural transition from monoclinic (*Cm*) to mixed (monoclinic (*Cm*) + Cubic (*Pm*-3*m*)) or pseudo-cubic to Cubic (*Pm*-3*m*) phase with increasing x. The SEM analysis show good crystallinity and the aggregation of micrometer-sized particles of about 2 µm. The magnetic phase transition from paramagnetic to G-type antiferromagnetic observed at or above RT for x = 0.6 and onwards, which also coincides with structural phase transition. The magnetic structure were found to be G-type antiferromagnetic for x = 0.6, 0.8 and 1.0. Magnetic hysteresis loops were observed for all the solid solutions and found that increasing x content the magnetic ordering has increased. The PFN_{1-x}-PFW_x solid solutions show systematic tuning of T_N with increasing x. The T_N of 155 K for x = 0.0 value increased systematically with x, to 194 K, 288 K, 295 K, 310 K and 350 K for, respectively. As like T_N, we expect the Curie temperature (T_C) of solid solution shift from 380 K (x=0.0) to 150 K (=1.0) with increasing x. The expected T_C for x=0.2, 0.4, 0.6, 0.8 and 1.0 is 310 K, 270 K, 220 K, 180 K

and 150 K, respectively. However for one or two samples, in this study, the T_N and T_C value might show near or above RT and hence may qualify as RT multiferroics. Further temperature dependent dielectric constant and ferroelectric studies are required to confirm the shifting of T_C. Mössbauer spectroscopy results show good agreement with magnetic properties of the samples measured through PPMS. The PFN shows paramagnetic doublet whereas sextet for PFW with antiferromagnetic ordering. By increasing x, the width of the line and isomer shift shows a systematic change. For x = 0.8 and 1.0 the spectra shows the sextet, confirms the existing antiferromagnetic order at RT and the origin of magnetism in the sample is due to the Fe^{3+}. Ferroelectric measurements show hysteresis with leaky behaviour. The increase of x in PFN_{1-x} - PFW_x is indirectly diluting the ferroelectric properties of PFN. The increased leaky behaviour with x is directly related to the increased Fe content with mixed valence and hence to the conductivity of the sample. Coexistence of biferroic nature i.e., ferroelectric and antiferromagnetic properties of PFN_{1-x} - PFW_x solid solutions open the possibility to explore this family of materials which may exhibit the magnetoelectric effect at near RT or RT and which show potential for future Pb based spintronics applications.

Acknowledgements

Authors (SM and BA) would like to acknowledge UGC-DAE-CSR, Mumbai Center for financial support through CRS-M-159 and CRS-M-200. Authors thank Dr. R Reddy, UGC-DAE-CSR, Indore Center (India) for providing P-E loop facility. Authors also acknowledge the DST-PURSE programme, Department of Physics, Bangalore University, Bangalore for the Raman facility.

References:

[1] M. Fiebig, Revival of the magnetoelectric effect, J. Phys. D 38 (2005) R123–R152.

[2] W. Eerenstein, N. D. Mathur, J. F. Scott, Multiferroic and magnetoelectric materials, Nature 442, (2006) 759 - 765.

[3] D. A. Sanchez, N. Ortega, A. Kumar, R. R. Malherbe, R. Polanco, J. F. Scott, R.S. Katiyar, Symmetries and multiferroic properties of novel room-temperature magnetoelectrics: Lead iron tantalate – lead zirconate titanate (PFT/PZT), AIP Adv. 1, (2011) 042169.

[4] N. A. Hill, Why are there so few magnetic ferroelectrics, J. Phys. Chem. B 104, (2000) 6694.

[5] G. A. Smolenskii, V.A. Bokov, V. A. Isupov, Physics of Ferroelectric Phenomena, Nauka, Leningrad (1987).

[6] Y. N. Venevtsev, V.V. Gagulin, V.N. Lyubimov, Ferroelectromagnets, Nauka, Moscow (1982), 2220 - 5.

[7] S. A. Ivanov, P. Nordblad, R. Tellgren, T. Ericsson, H. Rundlof, Structural, magnetic and Mössbauer spectroscopic investigations of the magnetoelectric relaxor $Pb(Fe_{0.6}W_{0.2}Nb_{0.2})O_3$ Solid State Sciences 9, (2007) 440 – 450.

[8] N. Kumar, A Ghosh, R. N. P. Choudhary, Electrical behaviour of $Pb(Zr_{0.52}Ti_{0.48})_{0.5}(Fe_{0.5}Nb_{0.5})_{0.5}O_3$ ceramics, Mater. Chem. Phys, 130, (2011), 381 – 386.

[9] J. F. Scott. Room temperature multiferroic magnetoelectrics, NPG Asia Mater, 5, 11, (2013), 72.

[10] D.M. Evans, A. Schilling, A Kumar, D. Sanchez, N. Ortega, M. Arredondo, R.S. Katiyar, J. M. Gregg, J. F. Scott, Magnetic switching of ferroelectric domains at room temperature in multiferroic PZTFT, Nat Commun, 4, (2013),1534.

[11] A. Dilsom, Sanchez, N. Ortega, A. Kumar, G. Sreenivasulu, R. S. Katiyar, J. F. Scott,

D. Evans, M. A. Arechavala, A. Schilling, J. M. Gregg, Room temperature single phase multiferroic magnetoelectrics: $Pb(Fe, M)_x(Zr,Ti)_{(1-x)}O_3$ [M= Ta, Nb]. J. Appl. Phys, 113, (2013), 074105.

[12]R. O. Cherifi, V. Ivanovskaya, L. C. Phillips, A. Zobelli, I. C. Infante, E. Jacquet, V. Garcia, S. Fusil, P. Briddon, N. Guiblin, A. Mougin, A. A. Ünal, F. Kronast, S. Valencia, B. Dkhil, A. Barthélémy, M. Bibes, Electric field control of magnetic order above room temperature, Nat Mat, 13, (2014), 345-351.

[13] D. M. Evans, A. Schilling, A. Kumar, D. Sanchez, N. Ortega, R. S. Katiyar, J. F. Scott, J. M.Gregg, Switching ferroelectric domain configurations using both electric and magnetic fields in Pb $(Zr,Ti)O_3$ - $Pb(Fe,Ta)O_3$ single-crystal lamellae. Phil. Trans. R. Soc. A, 372, (2014), 20120450.

[14] J. Schiemer, M. A. Carpenter, D. M. Evans, J. M. Gregg, A. Schilling, M. Arredondo, M. Alexe, D. Sanchez, N. Ortega , R. S. Katiyar, M. Echizen, E. Colliver, S. Dutton, J. F. Scott, Studies of the Room Temperature Multiferroic $Pb(Fe_{0.5}Ta_{0.5})_{0.4}$ $(Zr_{0.53}Ti_{0.47})_{0.6}O_3$, Resonant Ultrasound Spectroscopy, Dielectric and Magnetic Phenomena Adv. Funct. Mater, 24, (2014), 2993-3002.

[15] M. D. Glinchuk, E. A. Eliseev, A. N. Morozovska, New room temperature multiferroics on the base of single phase nanostructured perovskites. J. Appl. Phys. 116, (2014), 05410.

[16] M. D. Glinchuk, E. A. Eliseev, A. N. Morozovska. Theoretical description of anomalous properties on novel room temperature multiferroics $Pb(Fe_{1/2}Ta_{1/2})_x$ $(Zr_{0.53}Ti_{0.47})_{1-x}O_3$ and $Pb(Fe_{1/2}Nb_{1/2})_x(Zr_{0.53}Ti_{0.47})_{1-x}O_3$, J. Appl. Phys.119, (2016), 024102.

[17] S. Matteppanavar, B. Angadi, S. Rayaprol, Low temperature magnetic studies on $PbFe_{0.5}Nb_{0.5}O_3$ multiferroic, Physica B 448, (2014) 229 – 232.

[18] S. Matteppanavar, S. Rayaprol, A.V. Anupama, B. Angadi, B. Sahoo, Origin of room temperature weak-ferromagnetism in antiferromagnetic $Pb(Fe_{2/3}W_{1/3})O_3$ ceramic, Ceram Int. 41, 9, (2015) 11680 – 11686.

[19] J. Rodriguez-Carvajal, Recent advances in magnetic structure determination by neutron powder diffraction, Physica B 192 (1993) 55–69.

[20] R. A. Brand, Nucl. Instrum. Methods B 28, (1987), 398 - 402.

[21] R. N. P. Choudhary, D. K. Pradhan, C. M. Tirado, G. E. Bonilla, R. S. Katiyar, Relaxor characteristics of Pb $(Fe_{2/3}W_{1/3})O_3$-$BiFeO_3$ solid solution prepared by mechanosynthesis route, J. Appl. Phys. 100, 08, (2006) 4105.

[22] Bárbara Fraygola, José A. Eiras, Antiferromagnetic and Ferroelectric Phase Transitions and Instabilities in PFW-PT Multiferroic Solid Solution Characterized by Anelastic Measurement, Ferroelectrics, 448, (2013), 86–95.

[23] J. Lu, L. J. Qiao, P. Z. Fu, Y. C. Wu, Phase equilibrium of Bi_2O_3-Fe_2O_3 pseudo-binary system and growth of $BiFeO_3$ single crystal, J. Cryst. Growth 318, (2011) 936.

[24] K. Feng, L.-C. Wang, J. Lu, Y. Wu, B.-G. Shen, Experimentally determining the intrinsic center point of Bi_2O_3–Fe_2O_3 phase diagram for growing pure $BiFeO_3$ crystals, Cryst Eng Comm 15, (2013), 4900 - 4904.

[25] S. Matteppanavar, B. Angadi, S. Rayaprol, Single phase synthesis and room temperature neutron diffraction studies on multiferroic $PbFe_{0.5}Nb_{0.5}O_3$, AIP Conf. Proc. 1512, (2013) 1232 – 1233.

[26] S. Matteppanavar, S. Rayaprol, K. Singh, V. R. Reddy, B. Angadi, Evidence for magneto-electric and spin–lattice coupling in $PbFe_{0.5}Nb_{0.5}O_3$ through structural and magneto-electric studies, J Mater Sci 50, (2015), 4980 – 4993.

[27] S. Matteppanavar, B. Angadi, S. Rayaprol, Neutron diffraction studies on chemical and magnetic structure of multiferroic $PbFe_{0.67}W_{0.33}O_3$, AIP Conf. Proc. 1591, (2014), 1669 – 1671.

[28] N. Charoenthai, R. Traiphol, Progress in the synthesis of Ba $(Fe_{0.5}Nb_{0.5})O_3$ ceramics: A. versatile co-precipitation method, J Ceram Process Res. 12, 2, (2011), 191 – 194.

[29] S.A. Ivanov, S. G. Eriksson, N.W. Thomas, R. Tellgren, H. Rundlof, H A neutron powder diffraction study of the ferroelectric relaxor $Pb(Fe_{1/2}Ta_{1/2})O_3$, J. Phys. Condens. Matter 13, (2001) 25.

[30] J. R. Carvajal, BASIREPS: a program for calculating irreducible representations of space groups and basis functions for axial and polar vector properties; C. Ritter, (2011) Solid State Phenom. 170, (2007) 263.

[31] Z. G. Ye, K. Toda, M. Sato, E. Kita, H. Schmid, Synthesis, Structure and Properties of the Magnetically Ordered Relaxor Ferroelectric $Pb(Fe_{2/3}W_{1/3})O_3$, J. Korean Phys. Soc. 32, (1998) S1028.

[32] X. Hu, X. M. Chen, S.Y. Wu, Preparation properties and characterisation of CaTiO3modefied $Pb(Fe_{1/2}Nb_{1/2})O_3$, J. Eur. Ceram. Soc. 23, (2003) 1919 – 1924.

[33] A. K. Singh, D. Pandey, Evidence for MB and MC phases in the morphotropic phase boundary region of $(1-x)[Pb(Mg_{1/3}Nb_{2/3})O_3]-xPbTiO_3$: A Rietveld study, Phys. Rev. B 67, (2003) 064102.

[34] N. N. Luo, Q. Li, Z.G. Xia, X.C. Chu, You have full text access to this content Phase Diagram, Temperature Stability, and Electrical Properties of $(0.85-x)Pb(Mg_{1/3}Nb_{2/3})O_3$–$0.10Pb(Fe_{1/2}Nb_{1/2})O_3$–$0.05PbZrO_3$–$xPbTiO_3$ System, J. Am. Ceram. Soc. 95, (2012) 3246 – 3253.

[35] M. Zheng, Y. Hou, Z. Ai, M. Zhu, J. Appl. Phys. 116, (2014), 124110.

[36] E. F. Bertaut, Magnetism, ed G T Rado, H Shul (New York: Academic) chapter 4 (1963).

[37] S. Rayaprol, S. Mukherjee, S. D. Kaushik, S. Matteppanavar, B. Angadi, Electric field-induced tuning of magnetism in PbFe0.5Nb0.5O3 at room temperature, J. Appl. Phys. 118, (2015) 054103.

[38] D. P. Kozlenko, S. E. Kichanov, E. V. Lukin, N. T. Dang, L. S. Dubrovinsky, H.- P. Liermann, W. Morgenroth, A. A. Kamynin, S. A. Gridnev, B. N. Savenko, Pressure-induced polar phases in relaxor multiferroic $PbFe_{0.5}Nb_{0.5}O_3$, Phys. Rev. B 89, (2014) 174107.

[39] A. F. Garcıa-Flores, D. A. Tenne, Y. J. Choi, W. J. Ren, X. X. Xi, S. W. Cheong, Temperature-dependent Raman scattering of multiferroic $Pb(Fe_{1/2}Nb_{1/2})O_3$, J. Phys. Condens. Matter 23, (2010) 015401.

[40] O. Svitelskiy, J. Toulouse, G. Yong, Z. G. Ye, Polarized Raman study of the phonon dynamics in $Pb(Mg_{1/3}Nb_{2/3})O_3$ crystal, Phys. Rev. B 68, (2003) 104107.

[41] M. Zhu, C. Chen, J. Tang, Y. Hou, H. Wang, H. Yan,W. Zhang, J. Chen, W. Zhang, Effects of ordering degree on the dielectric and ferroelectric behaviors of relaxor ferroelectric $Pb(Sc_{1/2}Nb_{1/2})O_3$ ceramic, J. Appl. Phys. 103, (2008) 084124.

[42] A. Lebon, M. E. Marssi, R. Farhi, H. Dammak, G. Calvarin, Translational and orientational order in lead zinc niobate: An optical and Raman study, J. Appl. Phys. 89, (2001) 3947.

[43] E. Husson, L. Abello, A. Morell, Short-range order in $PbMg_{1/3}Nb_{2/3}O_3$ ceramics by Raman spectroscopy, Mater. Res. Bull. 25, (1990) 539.

[44] S. A. Prosandeev, E. Cockayne, B. P. Burton, S. Kamba, J. Petzelt, Y. Yuzyuk, R. S. Katiyar, B. S. Vakhrushev, Lattice dynamics in $PbMg_{1/3}Nb_{2/3}O_3$, Phys. Rev. B 70, (2004) 134110.

[45] N. Lampis, P. Sciau, A.G. Lehmann Rietveld refinements of the paraelectric and ferroelectric structures of $PbFe_{0.5}Nb_{0.5}O_3$, J. Phys. Condens. Matter 11, (1999) 3489.

[46] S. A. Ivanov, R. Tellgren, H. Rundlof, N. W. Thomas, S. Ananta, Investigation of the structure of the relaxor ferroelectric $Pb(Fe_{1/2}Nb_{1/2})O_3$ by neutron powder diffraction, J. Phys. Condens. Matter 12, (2000) 2393.

[47] Y. Yang, J. –M. Liu, H. B. Huang, W. Q. Zou, P. Bao, Z. G. Liu, Magnetoelectric coupling in ferroelectromagnet $Pb(Fe_{1/2}Nb_{1/2})O_3$ single crystals, Phys. Rev. B 70, (2004) 132101.

[48] B. Mihailova, R. J. Ange, A.-M. Welsch, J. Zhao, J. Enge, C. Paulmann, M. Gospodinov, H. Ahsbahs, R. Stosch, B. Güttler, U. Bismayer, Pressure-Induced Phase Transition in $PbSc_{0.5}Ta_{0.5}O_3$ as a Model Pb-Based Perovksite-Type Relaxor Ferroelectric, Phys. Rev. Lett. 101, (2008) 017602.

[49] B. Mihailova, B. Maier, C. Paulmann, T. Malcherek, J. Ihringer, M. Gospodinov, R. Stosch, High-temperature structural transformations in the relaxor ferroelectrics $PbSc_{0.5}Ta_{0.5}O_3$ and $Pb_{0.78}Ba_{0.22}Sc_{0.5}Ta_{0.5}O_3$, Phys. Rev. B 77, (2008) 174106.

[50] A. Kumar, R. S. Katiyar, Synthesis and Raman investigation of sol–gel-derived relaxor ferroelectric thin films, J. Raman Spectrosc, 38, (2007) 1307 – 1310.

[51] S. Gupta, R. S. Katiyar, R. Guo, A. S. Bhala, You have full text access to this contentStudy of structural phase transitions in solid-solution PZN $_{(1 - x)}$ – $_{x}$PT relaxor ferroelectric using Raman scattering, J. Raman Spectrosc, 31, 2000, 921.

[52] S. Matteppanavar, S. Rayaprol, A. V. Anupama, B. Sahoo, B. Angad, On the Room Temperature Ferromagnetic and Ferroelectric Properties of $Pb(Fe_{1/2}Nb_{1/2})O_3$, J Supercond Nov Magn, 28, 8, (2015) 2465 – 2472.

[53] A. K. Pradhan, K. Zhang, D. Hunter, J. B. Dadson, G. B. Loutts, P. Bhattacharya, R. Katiyar, J. Zhang, D. J. Sellmyer, U. N. Roy, Y. Cui, A. Burger, Magnetic and electrical properties of single phase multiferroic BiFeO3, J. Appl. Phys. 97, (2005) 093903.

[54] S. A. Larregola, J. C. Pedregosa, M. Alguero, R. Jimenez, M. Garcıa Hernandez, M. T. Fernandez-Dıaz, J. A. Alonso, Novel Near-Room-Temperature Type I Multiferroic: $Pb(Fe_{0.5}Ti_{0.25}W_{0.25})O_3$ with Coexistence of Ferroelectricity and Weak Ferromagnetism, Chem. Mater. 24, (2012) 2664.

[55] I. P. Raevskii, D. A. Sarychev, S. A. Bryugeman, L. A. Reznichenko, L. A. Shilkina, O. N. Razumovskaya, V. S. Nikolaev, N. P. Vyshatko, A. N. Salak, Crystallography Reports, 47, 6, (2002), 012 – 1015, Translated from 2002, Kristallografiya, 47, 6, (2002),1081–1084.

[56] Y. N. Venevtsev, V. V. SklyarevskiÏ, I. I. Lukashevich, 1976, Kristallografiya 21, 5, 971 [Sov. Phys. Crystallogr. 21, (1976) 556].

[57] G. S. Lotey, N. K. Verma, Structural, magnetic, and electrical properties of Gd-doped $BiFeO_3$ nanoparticles with reduced particle size, J. Nano Part. Res. 14, (2012) 742.

Highlights

- RT neutron diffraction studies on PFN_{1-x}-PFW_x (x = 0.0 to1.0) multiferroics
- Composition dependent changes in nuclear and magnetic structure.
- On increasing x, system exhibit a gradual phase transition from monoclinic to cubic
- Supporting Raman, magnetic, Mössbauer and ferroelectric studies
- Augmentation of Néel temperature (T_N) from 155 K to 350 K on increasing x